Supporting Information

Cobalt-based metal-organic framework derived Co/CoO@C under moderate temperature for improving the performance of photocatalytic degradation of organic pollutants

Yi-Lian Sun,[a†] Jia-Qi Wan,[a†] Ying He,[a] Bin Lv,[a] Shi-Yu Zhou,[a] Si-Tong Li,[a] Yu Liu,[a] Wen-Ze Li,*[a] Jian Luan,*[a] Xiao-Sa Zhang*[a]

College of Science, Shenyang University of Chemical Technology, Shenyang, 110142, P. R. China

E-mail: liwenze@syuct.edu.cn (W. Z. Li) jluan@syuct.edu.cn (J. Luan) xszhang@syuct.edu.cn (X. S. Zhang)

†These authors contributed equally to this work.

S1. Single crystal X-ray diffraction (SCXRD)

Crystallographic data for **Co-MOF** was collected using a Bruker SMART APEX II system with Mo Kα radiation (λ = 0.71073 Å) employing ω and θ scan modes; the structures were refined by full-matrix least-squares on F^2 using the SHELXTL software package,[S1] with crystal parameters, data collection parameters, and refinement details for the **Co-MOF** were summarized in Table S1, while the selected bond lengths and angles were listed in Table S2. The uncoordinated solvent water in the lattice were modelled as disordered over multiple positions. CCDC 2481426 for the **Co-MOF** was contained the supplementary crystallographic data in this paper. These data can be obtained free of charge from The Cambridge Crystallographic Data Centre *via* www.ccdc.cam.ac.uk/data_request/cif.

S2. Materials and measurements

All reagents and solvents were of analytical grade (≥99.0%). Fourier-transform infrared (FTIR) spectra were recorded in the range of 4000–500 cm^{-1} using a Varian 640-IR spectrometer with KBr pellets as the reference substance. Thermogravimetric (TG) curves were measured on a NETZSCH STA 449C thermogravimetric analyzer under a N_2 atmosphere from room temperature to 800 °C at a heating rate of 10 °C min^{-1} to evaluate the thermal stability of the **Co-MOF** sample. Powder X-ray

diffraction (PXRD) data were collected on a Rigaku diffractometer using Cu Kα radiation (λ = 1.5418 Å) over the 2θ range of 5–50° or 5–90° to distinguish the crystalline or amorphous phases of the **Co-MOF** and derived materials. The morphological characteristics of the materials were determined using scanning electron microscopy (SEM). The chemical composition, elemental states, and binding energies were analyzed by X-ray photoelectron spectroscopy (XPS) using a PerkinElmer 240C spectrometer with monochromatic Al Kα radiation. UV-Vis diffuse reflectance spectroscopy (DRS) data were acquired on a SP-1900 spectrophotometer across the wavelength range of 200 to 2500 nm.

S3. Evaluation of dye adsorption and photocatalytic performance

S3.1. Ultraviolet-visible diffuse reflectance spectra

Analyze the performance of the **Co-MOF** under solid-state UV conditions at room temperature using an ultraviolet spectrophotometer.

S3.2. Ultraviolet-visible spectra

The photocatalytic performance of the materials were evaluated by degrading 10 ppm aqueous solutions of GV, CR, MO, MB, and RhB. Initially, 50 mL of each of the five dye solutions was mixed with 10 mg of the synthesized carbon-based photocatalyst. The mixtures were magnetically stirred in the dark for 2 h to establish adsorption-desorption equilibrium, during which changes in absorbance were monitored using a UV-Vis spectrophotometer. After achieving adsorption equilibrium, the photodegradation process was initiated by irradiating the reaction systems in parallel using a visible-light source. (A 300 W xenon lamp with a 420 nm cut-off filter was used as the visible light source, and the light intensity was measured as 100 mW/cm^2 using a radiometer). Changes in the absorbance of the dye solutions were periodically monitored with the UV-Vis spectrophotometer during irradiation. Upon completion of each photocatalytic cycle, the photocatalyst was recovered via centrifugation, dried, and reused in further photocatalytic testing cycles.The degradation rates and kinetic characteristics of the photocatalyst for five dyes were studied. The formula is as follows:[S2]

$$\text{Degradation (\%)} = (C_0 - C_t)/C_0 \times 100 \qquad (1)$$

where C_t denotes the absorbance of the dye after irradiation and C_0 represents the initial absorbance of the dye, all experiments under photocatalytic conditions followed the Langmuir-Hinshelwood equation:[S3]

$$\ln(C_t/C_0) = -kt \qquad (2)$$

where C_t denotes the absorbance of the dye after irradiation, C_0 represents the initial absorbance of the dye, and k stands for the rate constant (min^{-1}); in the photocatalytic experiments for the reusable catalyst **Co/CoO@C-400**, the material was recovered after each absorbance measurement interval, dried at 60 °C, and reused in subsequent testing cycles.

Reference:

S1. P. Gall, T. Guizouarn and P. Gougeon, *Inorg. Chem.*, 2023, **62**, 6011–6019.

S2. B. Yan, N. Wang, Z. Sun, Y. Han, H. Meng, Y. Xu and X. Zhang, *CrystEngComm*, 2022, **24**, 8089–8098.

S3. M. Li, S. Yu and H. Huang, *Chinese J. Catal.*, 2024, **57**, 18–50.

Table S1 Crystallographic data for the **Co-MOF**.

Complex	**Co-MOF**
Empirical formula	$C_{39}H_{35}CoN_6O_{11}$
Formula weight	822.66
Temperature (K)	293(2)
Crystal system	Monoclinic
Space group	*P*21/*n*
a (Å)	11.4220(18)
b (Å)	13.846(2)
c (Å)	23.515(4)
α (°)	90
β (°)	94.321(5)
γ (°)	90
V (Å^3)	3708.2(10)
Z	4
Crystal size	0.17 × 0.15 × 0.13
ρ_{calc} (g cm^{-3})	1.474
μ (mm^{-1})	0.535
2θ Range (°)	4.092–56.686
F (000)	1704
R_{int}	0.0504
GOF	1.011
R_1[a] [$I > 2\sigma(I)$]	0.0460
wR_2[b] (all data)	0.1303

[a]$R_1 = \Sigma||F_o|-|F_c||/\Sigma|F_o|$, [b]$wR_2 = \Sigma[w(F_o^2-F_c^2)^2]/\Sigma[w(F_o^2)^2]^{1/2}$.

Table S2 Selected bond distances (Å) and angles (o) for the **Co-MOF**.

Co(1)–O(1)	2.0553(16)	Co(1)–N(1)	2.155(2)
Co(1)–O(4)#1	2.0912(15)	Co(1)–N(5)	2.176(2)
Co(1)–O(1W)	2.1176(19)	Co(1)–N(2)#2	2.207(2)
O(1)–Co(1)–O(4)#1	178.80(8)	O(1W)–Co(1)–N(5)	87.58(8)
O(1)–Co(1)–O(1W)	89.02(7)	N(1)–Co(1)–N(5)	177.69(8)
O(4)#1–Co(1)–O(1W)	89.85(7)	O(1)–Co(1)–N(2)#2	95.83(7)
O(1)–Co(1)–N(1)	92.10(7)	O(4)#1–Co(1)–N(2)#2	85.33(7)
O(4)#1–Co(1)–N(1)	87.50(7)	O(1W)–Co(1)–N(2)#2	172.60(8)
O(1W)–Co(1)–N(1)	90.12(8)	N(1)–Co(1)–N(2)#2	95.27(8)
O(1)–Co(1)–N(5)	88.09(7)	N(5)–Co(1)–N(2)#2	87.00(8)
O(4)#1–Co(1)–N(5)	92.27(7)		

Symmetry transformations used to generate equivalent atoms: #1 $x + 1$, y, z; #2 $–x + 1$, $–y$, $–z + 2$; #3 $x – 1$, y, z.

Table S3 The degradation rates of **Co/CoO@C-400/600/800/1000** against five dyes (GV, CR, MO, RhB and MB).

Material	Photocatalytic degradation rate (%)				
	GV	CR	MO	RhB	MB
Co/CoO@C-400	96.8	84.3	94.1	31.8	57.2
Co/CoO@C-600	95.0	70.5	85.2	13.1	22.6
Co/CoO@C-800	88.1	86.9	85.4	41.9	12.4
Co/CoO@C-1000	85.2	74.8	36.1	54.2	42.3

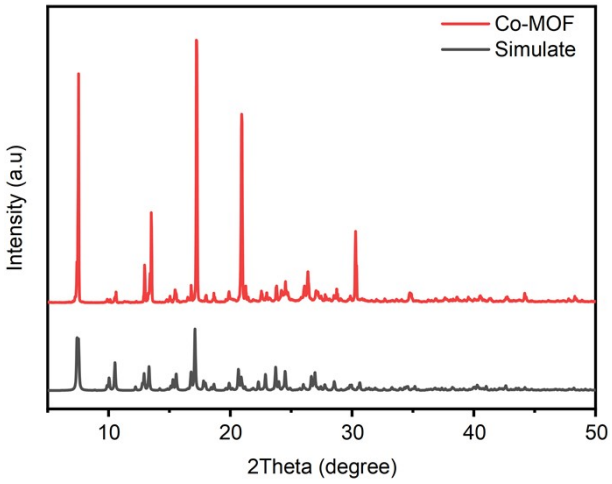

Fig. S1 The PXRD patterns of the **Co-MOF**.

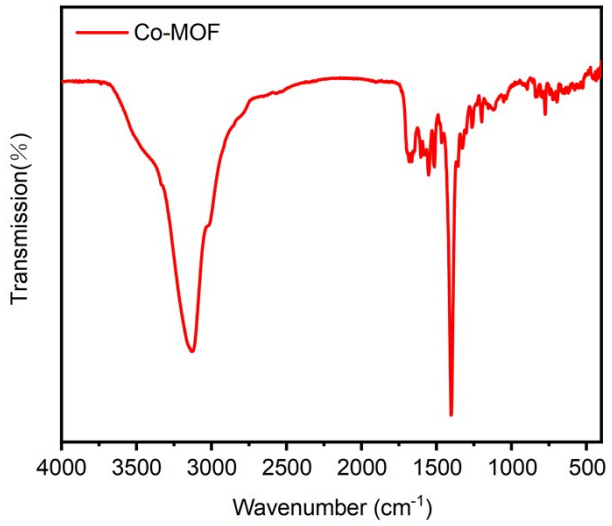

Fig. S2 The FTIR spectrum of the **Co-MOF**.

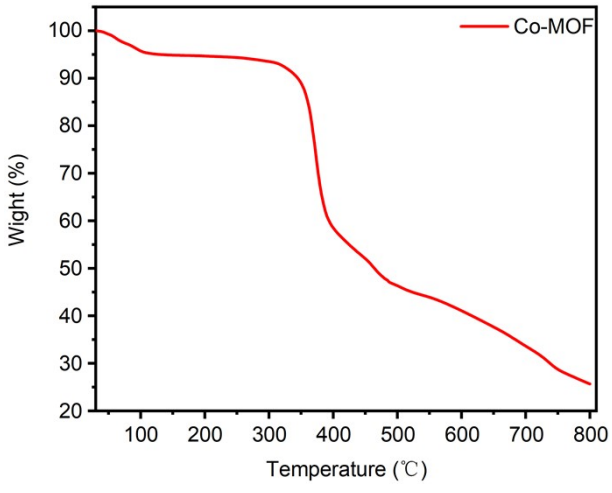

Fig. S3 The TG curve of the **Co-MOF**.

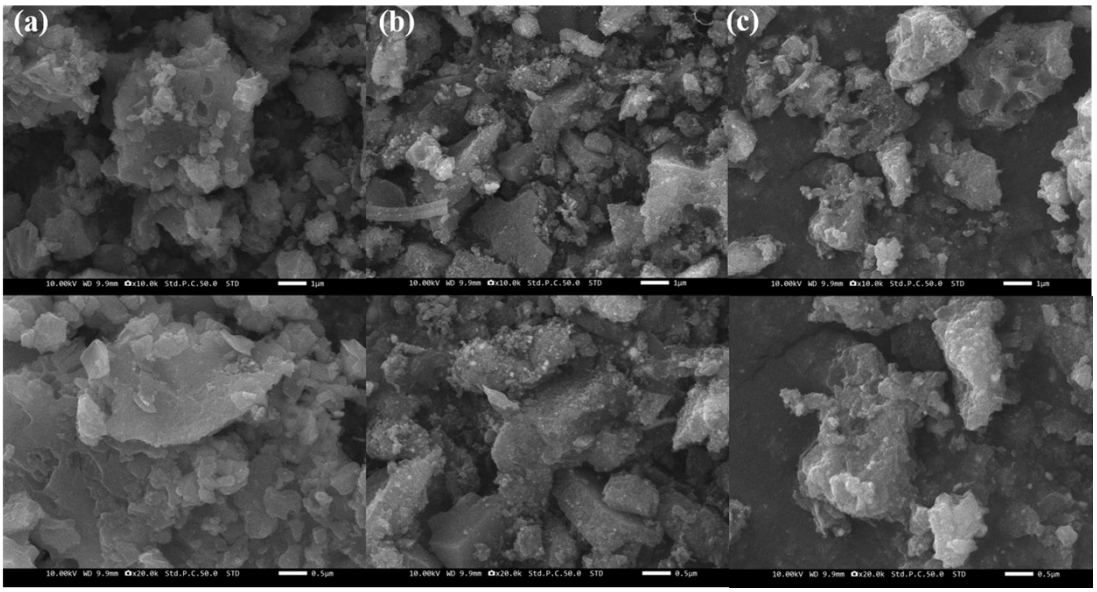

Fig. S4 SEM images of **Co/CoO@C-600** (a), **Co/CoO@C-800** (b) and **Co/CoO@C-1000** (c).

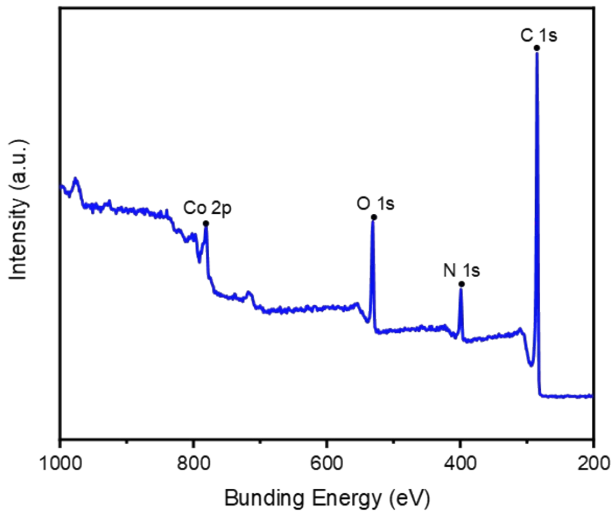

Fig. S5 High-resolution XPS spectrum of **Co/CoO@C-400**.

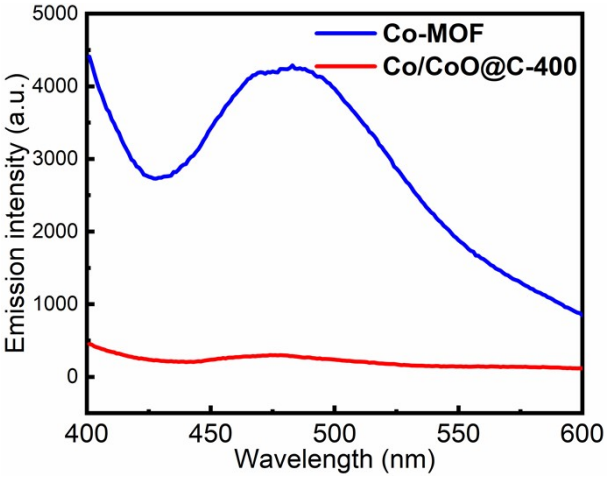

Fig. S6 The PL emission spectra **Co-MOF** and **Co/CoO@C-400**.

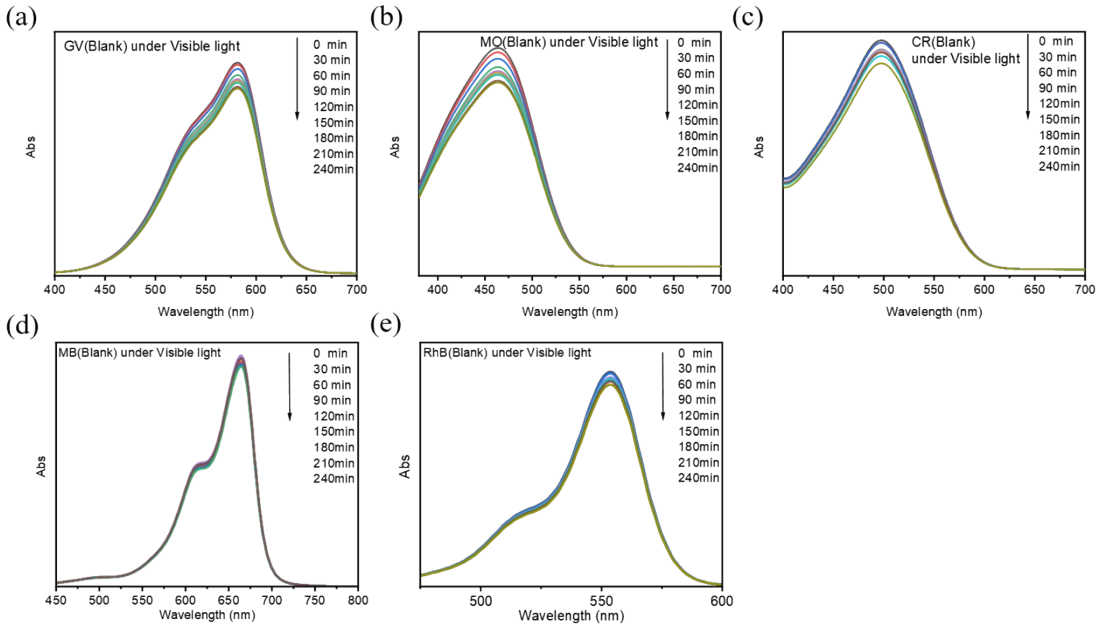

Fig. S7 UV-vis spectra of blank experiment (under visible light) for dye photocatalysis (performed in the absence of any catalyst).

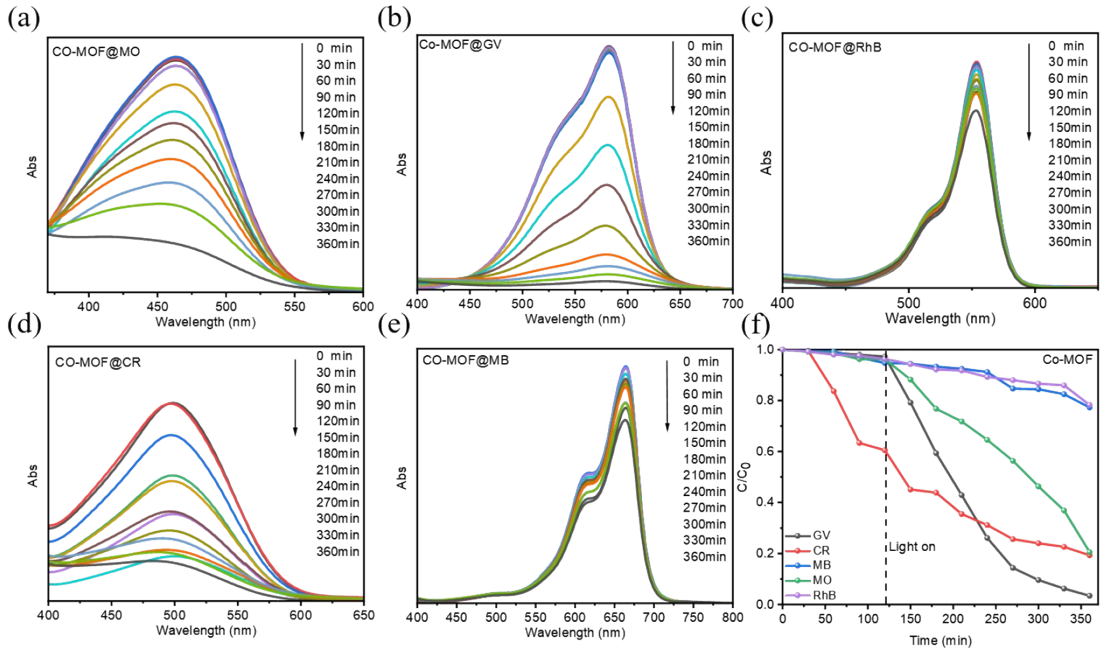

Fig. S8 The removal rate of MO (a), GV (b), RhB (c), CR (d), and MB (e) at different time points during exposure to the **Co-MOF**.(f) Recorded after different durations of photocatalytic degradation using **Co-MOF**.

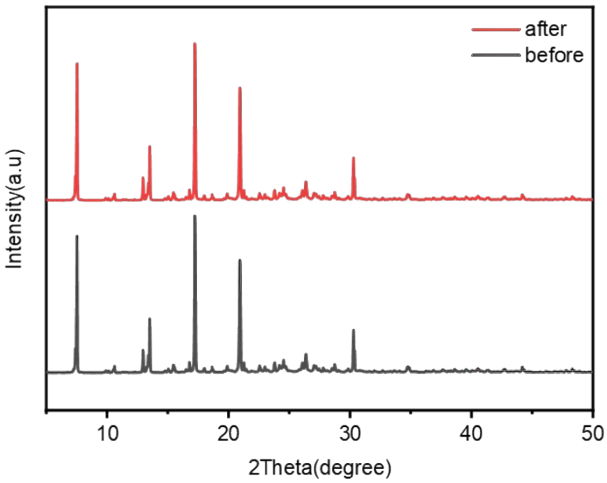

Fig. S9 Comparison of PXRD between raw **Co-MOF** and after four cycles of testing.

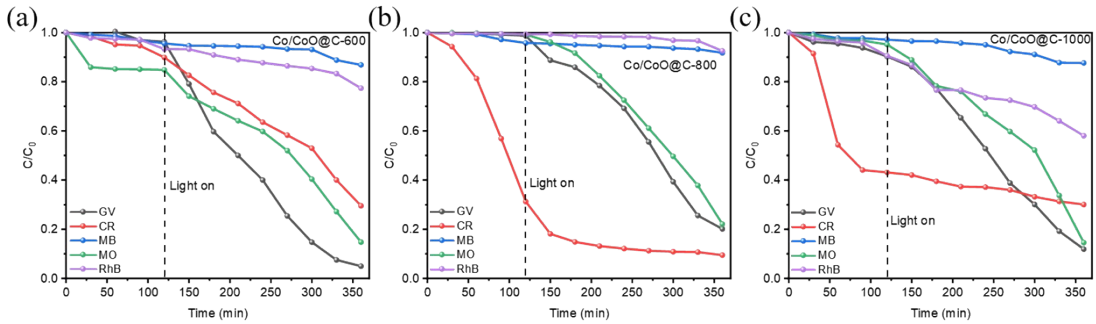

Fig. S10 Photocatalytic degradation curves of GV, CR MB, MO, and RhB with **Co/CoO@C-600/800/1000**.

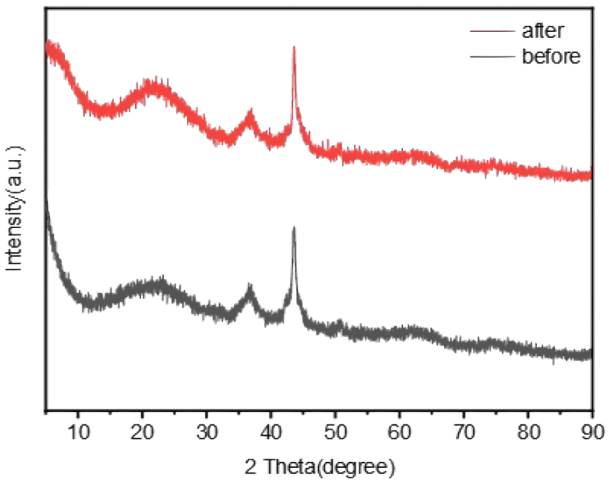

Fig. S11 PXRD patterns of **Co/CoO@C-400** before and after the photocatalytic reaction.

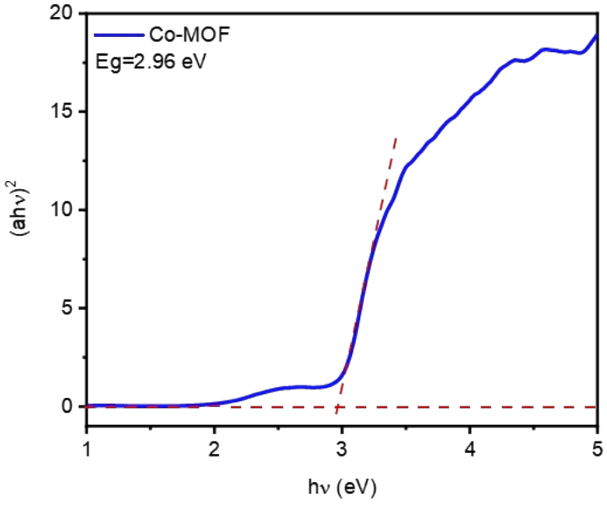

Fig. S12 The Tauc plots corresponding to the **Co-MOF**.